

**Crystallization and unusual rheological behavior in poly(ethylene oxide)-clay
nanocomposites**

Antonios Kelarakis and Emmanuel P. Giannelis

Department of Materials Science and Engineering, Cornell University, Ithaca, NY 14853

Abstract

We report a systematic study of the crystallization and rheological behavior of poly(ethylene oxide) (PEO) clay nanocomposites. To that end a series of nanocomposites based on PEOs of different molecular weight ($10^3 < MW < 10^5$ g/mol) and clay surface modifier was synthesized and characterized. Incorporation of organoclays with polar (MMT-OH) or aromatic groups (MMT-Ar) suppresses the crystallization of polymer chains in low MW PEO, but does not significantly affect the crystallization of high MW matrices. In addition, the relative complex viscosity of the nanocomposites based on low MW PEO increases significantly, but the effect is less pronounced at higher MWs. The viscosity increases in the series MMT-Alk < MMT-OH < MMT-Ar. In contrast to the neat PEO which exhibits a monotonic decrease of viscosity with temperature, all nanocomposites show an increase after a certain temperature. This is the first report of such dramatic enhancements in the viscoelasticity of nanocomposites, which are reversible, are based on a simple polymer matrix and are true in a wide temperature range.

Keywords: organoclays, poly(ethylene oxide), nanocomposites, crystallization, rheology

1. Introduction

Unlike conventional binary systems, nanocomposites do not generally follow classic micromechanic modeling due to the significant contribution of the interfacial zone in which the polymer chain and structure dynamics are dramatically altered (1-3). Consequently, the nature and the extent of the interfacial zone have a pivotal role on the macroscopic properties of the nanocomposites. The potentially large organic-inorganic interfacial area can be realized (and, thus, exploited) only when the matrix-filler interactions are sufficiently strong to overcome the inherent tendency of nanoparticles for self-aggregation (4). Thus far, the common practice to optimize the performance of nanocomposites can be described as a series of “trial and error” efforts for selected matrix-filler combinations, while bottom up approaches are only recently emerging.

In the case of clay nanocomposites, the affinity of nanofillers to a given polymer matrix is improved by proper modification of the platelets by ion-exchange reactions that typically replace the native ions of pristine clay with ammonium cations bearing hydrocarbon chains with tunable length and composition (5). This strategy has been applied to promote clay dispersion and even exfoliation in the polymer matrix by altering the enthalpy contribution of host/guest interactions and by expanding the interlayer distance. That being said it is instructive to note that complete exfoliation is not a prerequisite for performance enhancements. In fact, intercalated clay hybrids often exhibit improved properties in terms of thermomechanical behavior, dimensional stability, fire retardancy, and barrier characteristics (6-12).

Oftentimes organoclay/polymer hybrids are melt-processed using techniques such as extrusion and injection molding (6-12), without the need of any solvent. For melt-processed nanocomposites, it is the interplay between the strength of polymer matrix-nanoparticle interactions, the rheological response and the level of dispersion that defines the structure and dynamics of the system. Strong polymer- clay interactions give rise to enhanced local flow disturbance forces that prevent further polymer diffusion. Therefore, the rheological response of clay hybrids apart from being directly related to their

processability and, thus, applicability, can provide insights into the particle-polymer interactions (13,14) while functioning as a decisive parameter for microstructure evolution (8,15,16).

By virtue of its hydrophilicity poly(ethylene oxide), PEO, exhibits a certain degree of affinity to the silicate surface, even in the absence of any surface modifier. For that reason, PEO based clay nanocomposites have long been considered as model systems to study the mechanism and the implications of polymer confinement within the narrow interlayer gallery (17-29). In addition, PEO nanocomposites are promising candidates as electrolytes for solid state batteries given that they exhibit superior ionic conductivity (17-20,22-24), in a manner that is directly related to their chain conformation (21-26,29), crystallization (19,20,22,26) and rheological/mechanical properties (27-29).

The present study represents the first systematic investigation that focuses on elucidating the dependence of crystallization and flow behavior in a series of PEO based clay nanocomposites (18 in total) with respect to polymer molecular weight and the nature of the clay surface modifier. Particular emphasis is given to the origin of the highly unusual (in terms of strength, steepness and thermal reversibility) viscoelastic enhancements observed at elevated temperatures. To that end, we study the rheological behavior of the hybrids at temperatures as high as 120 °C above their melting point, e.g. within a region rarely investigated.

2. Experimental

2.1. Preparation of the nanocomposites

α - ω hydroxyl-terminated poly(ethylene oxide), with weight average molecular weights (MW) 1×10^3 , 8×10^3 , 2×10^4 and 1×10^5 g/mol were purchased from Polysciences Inc, while an additional grade with MW= 2×10^3 g/mol was acquired from Sigma-Aldrich Co. Poly(ethylene glycol) dimethyl ether, MW= 4.2×10^4 g/mol was provided from

Polysciences Inc, and is abbreviated hereafter as dimethyl-PEO. Three commercial organically modified montmorillonites (MMT) clays were used: I.30T from Nanocor Inc. which is octadecyltrimethyl ammonium-substituted MMT (MMT-Alk), Cloisite 30B from Southern Clay Products, a bis(hydroxyethyl)methyl tallow ammonium-exchanged MMT (MMT-OH), and Perchem 97 from Southern Clay Products that is modified with benzyltallowdimethylammonium (MMT-Ar). Repeated washings with ethanol-water solution was used to remove any excess of ammonium ions. Prior to the preparation of the nanocomposites, the components were dried in a vacuum oven overnight before being physically mixed. The concentration of clay particles was 5 wt % in all nanocomposites. The nanocomposites were prepared by melt intercalation (90 °C for 4 h followed by 160 °C for 2 h under nitrogen). PEO 1×10^3 /MMT-Ar refers to the hybrid based on PEO with MW= 1×10^3 g/mol and contains 5 wt% of MMT-Ar nanoclay. Similar notations are adopted for the various hybrids throughout the text.

2.2. Methods

Differential scanning calorimetry (DSC) thermographs were collected on a TA Instrument Q1000 series calorimeter over the temperature range -100 to 100 °C at a scan rate at 10 °C/min. A heat-cool-heat sequence was followed and the results presented below are for the first cooling (crystallization temperature, T_{cr}) and the second heating (melting temperature, T_m) scans, respectively. At the end of the first heating (data not shown here) the samples were kept at 100 °C for 10 min to erase any thermal history.

The rheological properties of the nanocomposites were determined using a Paar Physica Modular Compact Rheometer 300 (MCR 300) equipped with parallel plate geometry (diameter 25 mm). Measurements were performed in small amplitude oscillatory shear in a dry nitrogen atmosphere to suppress oxidative degradation. The frequency scans typically covered a range of angular frequency (ω) from 0.1 to 100 rad s^{-1} . The temperature sweeps were recorded at a rate of 1 °C/min at $\omega=10$ rad s^{-1} . Before any measurement the samples were kept for 0.5 h at 160 °C in the rheometer to thermally equilibrate and relax structurally.

3. Results and Discussion

3.1 Morphology and thermal properties

TEM images of selected samples show that mixing PEO with silicate clay leads to intercalated nanocomposites consistent with previous studies (19-29). Based on x-ray diffraction (XRD) measurements all samples showed an intercalated structure with d-spacing between 34-37 Å. The d-spacing of MMT-Ar, MMT-Alk, and MMT-OH with PEO (MW=1x10³ g/mol) is 34, 35.3, and 36.8 Å, respectively. The corresponding values for the nanoclays in the absence of the polymer are 19.6, 17.1 and 18.4 Å, respectively. A number of earlier studies have reported a d-spacing of 17±1 Å for PEO/pristine smectite clays intercalates prepared either by melt compounding (19-22) or by solution-assisted blending (22-24). It was found that for “polymer-rich” hybrids, the basal spacing is insensitive to the MW of the polymer. The d-spacing has been correlated with a single intercalated layer of PEO in a helical conformation (23) or a disordered double-layer (24,25). Intercalation of PEO with MW in the range 10⁵-10⁶ g/mol in organically modified nanoclays results in higher d-spacing values, oftentimes in the range of 34±4 Å (26-29) in agreement with the values reported above.

Melting/crystallization studies are crucial in assessing the macroscopic properties of nanocomposites given that rigid inorganic particles (of both nano- and micro dimensions) embedded within a variety of polymers can typically provide heterogeneous nucleation sites that facilitate crystallization (30,31) or can preferentially promote the development of a certain crystalline phase in polymorphic matrices (32-34). As seen in Figure 1, addition of the different nanoclays in PEO with a molecular weight of 1x10³ g/mol affects both the melting, T_m, and crystallization, T_{cr} temperatures. MMT-Alk seems to have the smallest effect on the crystallization of PEO. MMT-Ar and MMT-OH lower the T_m by ~ 5 °C and T_{cr} by ~ 7 and 14 °C, respectively. At the same time, the enthalpy of fusion (ΔH_{fus}) drops from 138 J/g for the neat matrix, to 108 J/g for PEO1x10³/MMT-Ar and 90 J/g for PEO1x10³/MMT-OH. The changes in T_m and T_{cr} are present in hybrids

based on polymers with higher MW, although the effect seems to be diminishing at higher MWs (Figure 2). T_m and T_{cr} of hybrids based on PEO with MW 1×10^5 g/mol are virtually the same compared to the neat polymer.

It has been reported that incorporation of organoclays into PEO (MW in the range 1×10^5 - 6×10^5 g/mol) caused an initial increase in both T_m and crystallinity followed by a decrease upon further clay addition (29). A monotonic (though not pronounced) decrease in T_m and the corresponding heat of fusion with increasing nanoclay loading was observed elsewhere (28,35). In another study the heat of fusion of PEO with MW of 1×10^5 g/mol was found to increase with organoclay content higher than 4 wt% regardless of the polarity of the surface modifier (36). Lastly, it has been reported that neither MMT-OH nor MMT-Alk had any major effect on the crystallization of PEO with MW= 1×10^5 g/mol (37). Within this somewhat conflicting background, the present systematic study provides detailed information about the crystallization behavior of PEO nanocomposites. Our data suggests that clay affects most the crystallization of low MW PEO. For these systems the degree of crystallinity follows the order: neat polymer > MMT-Alk > MMT-OH > MMT-Ar.

Suppression of crystallization of PEO due to the inclusion of pristine clay layers (20,22,25,26,38,39), single-walled carbon nanotubes (40,41), plasticizers (42,43) or small ionic species (44) has been reported previously. The amorphization of PEO in the vicinity of pristine (not surface modified) silicate clays (39) has been attributed to coordination of alkali ions (Na^+ or Li^+) to ethylene oxide units that gives rise to crown ether type backbone conformation and defects in the helical conformation of PEO chains (43-45). In the present study, the bulky character and chemistry of the organic surfactants does not favor similar coordination interactions. Instead, the suppressed crystallization observed especially for the low MW PEO based hybrids can be attributed to steric hindrance or confinement effects imposed to polymer chains by the nanoclay. The extent of confinement largely depends upon the strength of polymer-nanoparticle interactions and, thus, is sensitive to the nature of the surfactant. However, the presence of clay and

the type of surface modifier don't have much of an effect in strongly crystallizable (with a multi-folded motif) high MW PEO matrices.

3.2 Rheological behavior

3.2.1 Effect of molecular weight of the matrix and the nature of surfactant

The small-amplitude oscillatory frequency scan of the neat PEO melt (MW= 8×10^3 g/mol) at 75 °C is consistent with a predominantly viscous polymer (Figure 3). In contrast, all nanocomposites exhibit a pseudo solid-like response. In addition, within the entire rheological window the storage modulus is higher compared to those of the neat polymer. The storage modulus, G' , for the different surface-modified clays increases in the order MMT-Alk < MMT-OH < MMT-Ar. The crossover frequency of the storage and loss modulus (G' and G'' , respectively), follows a similar trend suggesting that the contribution of the non-terminal relaxation mode is highest in the MMT-Ar clay. The significant deviations from the ideal melt behavior and the evolution of a non-terminal mode, which appears to be present in all hybrids, can be attributed to the formation of a physically interconnected network of nanoparticles (15,16,46-49). Similar behavior was observed for all nanocomposites studied but the effect was much smaller in hybrids based on PEO with MW= 1×10^5 g/mol.

That MMT-Alk affects the least the rheology is consistent with having the weakest interactions between the PEO and the clay nanoparticles in that system. Note that PEO interacts favorably with the silicate layers but unfavorably with the aliphatic surface modifier. In contrast, hydrogen bonding between the ether oxygen of the PEO and the hydroxyl groups of the surface modifier in PEO/MMT-OH hybrids is expected to influence significantly the rheology. The even larger effect observed in the PEO/MMT-Ar hybrids was somewhat unexpected based on polarity arguments alone. However, it is consistent with the large negative value of Flory-Huggins interaction parameter, χ , in the PEO/benzene binary system (50), which is due to specific charge transfer interactions between the benzene and the EO repeat units.

The relative complex viscosity (η_{rel}^*) at $T=75\text{ }^\circ\text{C}$ ($\eta_{rel}^* = \eta_{hybrid}^* / \eta_{matrix}^*$, where η_{hybrid}^* and η_{matrix}^* , are the complex viscosities of the nanocomposite and the PEO polymer matrix, respectively) of the various hybrids is plotted as a function of the MW of the polymer in Figure 4. This representation provides a comprehensive comparison of the flow characteristics of all systems. The data plotted refer to $\omega=0.1\text{ s}^{-1}$, e.g. the lowest angular frequency studied that better approximates the static behavior (zero shear limit) of the various systems. Consistent with the trends for G' for hybrids based on PEO with a $MW = 8 \times 10^3\text{ g/mol}$ seen in Figure 3, the relative complex viscosity also increases in the series $MMT\text{-Alk} < MMT\text{-OH} < MMT\text{-Ar}$. The same is true for hybrids based on PEO with MW of 1×10^3 and $2 \times 10^3\text{ g/mol}$. The increase in complex viscosity becomes less pronounced for the hybrids based on PEO with a MW of $2 \times 10^4\text{ g/mol}$ and virtually disappears when the MW becomes $1 \times 10^5\text{ g/mol}$. As before, we attribute the trends in complex viscosity for the lower MW PEOs to the increasing interactions between the polymer and the nanoclay. However, as the MW of the polymer progressively increases, contributions of the polymer chain entanglements start to gradually dominate the rheology. Note that the critical entanglement molecular weight for PEO (denoted by the dashed line in Figure 4) is $4.4 \times 10^3\text{ g/mol}$ (51).

3.2.2. Effect of temperature

The temperature dependence of complex viscosity (η^*) for nanocomposites based on PEO with $MW=8 \times 10^3\text{ g/mol}$ during a single frequency cooling sweep ($\omega=10\text{ s}^{-1}$) is plotted in Figure 5. (The isochronal temperature scans presented in Figure 5 were performed at an intermediate angular frequency $\omega=10\text{ s}^{-1}$, given that very high frequency ramps cannot adequately approximate the zero shear behavior, while very low frequency ramps require considerable time, jeopardizing the structural stability of the systems). It can be seen that η^* of the neat matrix monotonically increases upon cooling as expected for a typical polymer melt. In contrast, η^* of the nanocomposites initially decreases and then increases as the temperature continues to decrease. The viscosity of $PEO_{8 \times 10^3}/MMT\text{-Ar}$ has a maximum value $\eta^*=3.1\text{ kPa s}$ at $160\text{ }^\circ\text{C}$, goes through a

minimum $\eta^*=0.8$ kPa s at 112 °C and returns to a value of $\eta^*=1.1$ kPa s at 75 °C. Similarly, η^* of PEO 8×10^3 /MMT-OH and PEO 8×10^3 /MMT-Alk exhibits minimum values close to 140 °C. The trend for the complex viscosity we observed in Figure 4 for 75 °C (PEO < PEO/MMT-Alk < PEO/MMT-OH < PEO/MMT-Ar) appears to hold for the entire temperature range considered (75 - 160 °C). Similar increases in η^* at high temperatures were observed for the other hybrids, except for those based on PEO with MW= 1×10^5 g/mol.

Figure 6a shows the frequency dependence of G' and G'' for PEO 8×10^3 /MMT-Ar at 75 and 160 °C. At low frequencies G' is higher at 160 °C compared to that at 75 °C opposite of what is expected for an ideal melt. In other words the pseudo-solid character of the hybrid is more pronounced at 160 °C, as G' becomes almost invariant with frequency. Similarly, η^* shows a crossover at 4 s^{-1} (Figure 6b) i.e. the increased viscosity at higher temperatures is limited to the low frequency region. In this system the non-terminal relaxation mode, which is the signature of a well-interconnected microstructure, is more pronounced at 160 °C.

To further elucidate the mechanism of the rheological behavior and the role of hydrogen bonding we considered a MMT-Ar nanocomposite based on a PEO dimethyl ether (abbreviated as dimethyl-PEO). Due to the complete absence of hydroxyl groups in this system, there is no possibility for hydrogen bonding between polymer-clay or polymer-polymer. The rheograms of dimethyl-PEO/MMT-Ar plotted in Figure 7 show that G' and η^* are 20-times higher at 160 °C compared to 75 °C. More importantly the high temperature reinforcement is apparent within the entire frequency window (as opposed to the crossover behavior seen in Figure 6). These results suggest that hydrogen-bonding is not a precondition for the rise in viscosity observed at elevated temperatures. To the best of our knowledge, such dramatic enhancements in the viscoelasticity of nanocomposites, which are reversible, are based on a simple polymer matrix and are true in a wide temperature range have not been reported to date.

Below we compare our results with what has been reported before and we highlight some unique aspects about the behavior of our system. Previously the high-temperature viscosity rise in clay hybrids has been attributed to temperature induced order-disorder (52) or to a nematic-isotropic transition (53) of the polymer matrix itself. In the present study, however, since the viscosity of the neat polymer melt monotonically decreases with temperature (Figure 5), the possibility of major structural rearrangements of the matrix itself can be ruled out.

Non-typical increases in storage modulus with temperature have been also observed during aging (so called “ripening”) of clay hybrids due to polymer migration within the clay galleries as the system approaches an equilibrium microstructure (54,55). At the end of the first heating/cooling cycle the hybrids appear to be irreversibly stiffened and further thermal treatment does not impart additional stiffening (54). In contrast, the viscosity changes observed in this study are thermally reversible. Figure 8 displays the rheograms of PEO₂×10³/MMT-Ar during cooling and subsequent heating. Despite the hysteresis between the cooling and heating scans, the viscosity increases reversibly at elevated temperatures. In fact, after 10 min of thermal annealing at 160 °C, η^* closely approaches the value measured at the beginning of the thermal cycle. Thus, the highly unusual rheological behavior reported here cannot be attributed to “ripening”, which is an inherently irreversible process.

In another report, clay nanocomposites based on poly(ethylene-co-vinyl acetate) and poly(ethylene-co-methyl acrylate) were seen to undergo liquid to solid-like transition upon heating, but only at temperatures higher than 200 °C, where significant decomposition of surfactant has been detected (56). Thus, the decomposition of surfactant was thought to be responsible for the unusual rheological trends. In contrast, surfactant decomposition is not a concern in this study, given that the effects commence for certain systems at 112 °C (Figure 5), e.g. at a temperature far below the onset decomposition temperature of organically modified silicates estimated to be around 180 °C (57).

Lastly in a series of investigations Lee and Han described in much detail the low frequency/high temperature rheological changes observed for selected clay nanocomposites based on polycarbonate/MMT-OH (58), polystyrene-block-hydroxylated polyisoprene/MMT-OH (50), poly(ethylene-co-vinyl acetate)/non polar MMT and poly(ethylene vinyl alcohol)/MMT-OH (60). The authors attributed this behavior to the better exposure of the platelets to the polymer chains at high temperatures (and thus stronger interactions), while emphasizing the importance of hydrogen-bonding between particles and polymer chains for certain systems. In our work the strongest effect was observed in nanocomposites based on dimethyl-PEO and MMT-Ar (i.e. in a system lacking hydrogen-bonding interactions). At the same time the effect was absent in PEO 1×10^5 /MMT-OH, where hydrogen-bonding is possible but the MW of the polymer is high.

Based on the above discussion, it is clear that an underlying mechanism different in origin than those described previously in the literature might account for our results. The dramatic and steep change in rheology with temperature implies the evolution of a percolated microstructure (at least in a localized level) above a critical temperature. Although, a generalized model to account for the formation of a rigid network in a diverse range of molten nanocomposites has still to emerge, it is clear that the development of such a network relies on topological, energetic as well as kinetic factors.

A percolated network with solid-like behavior can be established through interparticle physical connectivity, ideally in an edge-to-face fashion for clay delaminated layers (if at all present) or small tactoids. Given that the TEM images of the quenched nanocomposites (after being subjected to thermal annealing at 160 °C) do not support the development of a continuous network of nanoparticles, we attribute the unusual rheological effects to the reorganization of the polymer chains rather than the nanoparticles themselves. Critical for the network formation is the strength of the interactions between the polymer chains and the nanoparticles, that are primarily controlled by enthalpic factors. The thermoreversible character of the rheological enhancements underscores the vital role of the interactions. It has been suggested that the

absorbed polymer chains not only increase the effective filler volume fraction in the system (facilitating percolation) but can also function as bridges between neighboring nanoparticles (47,61). In that sense, the inherent compatibility of PEO with the silicate layers but more importantly the affinity of the polymer chains to the surface modifier contribute significantly to the rheological behavior. Embedded in a highly viscous environment (such as PEO with $MW=1 \times 10^5$ g/mol) the polymer chains and the nanoparticles are kinetically trapped and, thus, lack mobility for any major structural rearrangement. In other words, sufficient level of internal fluidity constitutes a necessary condition for the reorganization of the polymer chains and/or nanoparticles and the thermal relaxation of the hybrid systems. When this requirement is fulfilled, dispersed nanoparticles with strong affinity to the matrix (here the sequence seems to be MMT-Alk < MMT-OH < MMT-Ar) facilitate the formation of a percolated network at higher temperatures giving rise to highly unusual rheological signatures.

Conclusions

Incorporation of organoclays significantly suppresses crystallization in low and moderate MW poly(ethylene oxide), but the effect is diminished for high molecular weight matrices. The substantial rise in melt viscosity observed in the presence of MMT-Ar and MMT-OH organoclays can be traced back to favorable thermodynamic interactions between PEO chains and clay surface modifiers. Increasing the MW of the matrix leads to an enhanced contribution of the polymer chain entanglements to the overall rheological response that gradually undermines the impact of nanoclays. At elevated temperatures, the nanocomposites exhibit dramatic increases in viscoelasticity. In certain hybrids the storage modulus is as much as twenty times higher at 160 °C compared to the value at 75 °C. This highly unusual effect, in terms of strength, steepness and thermal reversibility seems to be correlated with the internal fluidity of the system (thus the molecular weight and the end group chemistry of the matrix) and the level of polymer-nanoparticle interactions (governed by the chemistry of the surface modifier on the clay).

Acknowledgements

This material is based on work supported as part of the Energy Materials Center at Cornell, an Energy Frontier Research Center funded by the U.S. Department of Energy, Office of Science, Office of Basic Energy Sciences under Award Number DE-SC0001086. This publication is based on work supported in part by Award No. KUS-C1-018-02, made by King Abdullah University of Science and Technology (KAUST).

Figures

Figure 1. DSC thermographs of 5wt% clay nanocomposites based on PEO with MW=1x10³ g/mol.

Figure 2. Melting (open symbols) and crystallization (filled symbols) temperature of PEO nanocomposites compared to the corresponding neat matrices with various molecular weights.

Figure 3. Frequency dependence of the storage (filled symbols) and loss (open symbols) modulus of nanocomposites based on PEO with MW=8x10³ g/mol at 75 °C.

Figure 4. Relative complex viscosity (η^*_{rel}) at 75 °C of the poly(ethylene oxide) based nanocomposites versus the MW of the matrix. Dashed line represents the critical entanglement molecular weight for PEO (MW=4.4x10³ g/mol).

Figure 5. Temperature dependence of complex viscosity (η^*) of nanocomposites based on PEO with MW=8x10³ g/mol during isochronal cooling ramps ($\omega= 10 \text{ s}^{-1}$, cooling rate 1 °C/min).

Figure 6. Frequency dependence of; (a) the storage (filled symbols) and loss (open symbols) modulus and (b) complex viscosity η^* for 5 wt% MMT-Ar nanocomposites based on PEO (MW=8x10³ g/mol) at 75 °C (blue squares) and 160 °C (red circles).

Figure 7. Frequency dependence of; (a) the storage (filled symbols) and loss (open symbols) modulus and (b) complex viscosity η^* for nanocomposites based on dimethyl-PEO (MW=4.2x10⁴ g/mol) at 75 °C (blue squares) and 160 °C (red circles).

Figure 8. Temperature dependence of complex viscosity (η^*) of 5 wt% MMT-Ar nanocomposites based on PEO with MW=2x10³ g/mol during an isochronal cooling (blue circles)/heating (red squares) cycle ($\omega= 10 \text{ s}^{-1}$, cooling/heating rate 1 °C/min).

References

1. Ji XL, Jing JK, Jiang W, Jiang BZ. *Polymer Engineering and Science* 2002;42:983-993
2. Rao YQ, Pochan JM. *Macromolecules* 2007;40:290-296
3. Al-Ostaz A, Pal G, Mantena PR, Cheng A. *Journal of Materials Science* 2008;43:164-173
4. Coleman JN, Khan U, Gun'ko YK. *Advanced Materials* 2006;18: 689-706
5. de Paiva LB, Morales AR, Diaz FRV. *Applied Clay Science* 2008;42:8-24
6. Giannelis EP. *Advanced Materials* 1996;8:29-35
7. Le Baron PC, Wang Z, Pinnavaia TJ. *Applied Clay Science* 1999;15:11-29
8. Ray SS, Okamoto M. *Progress in Polymer Science* 2003; 28:1539-1641
9. Nguyen QT, Baird DG. *Advances in Polymer Technology* 2006;25:270-285
10. Okada A, Usuki A. *Macromol. Mater. Eng.* 2006;291:1449-1476
11. Paul DR, Robenson LM. *Polymer* 2008;49:3187-3204
12. Pavlidou S, Papaspyrides CD. *Progress in Polymer Science* 2008;33:1119–1198
13. Wagener R, Reisinger TJC. *Polymer* 2003;44:7513-7518
14. Vermant J, Ceccia S, Dolgovskij MK, Maffettone PL, Macosko CW. *J. Rheol.* 2007; 51:429-450
15. Krishnamoorti R, Giannelis EP. *Macromolecules* 1997;30:4097-4102
16. Krishnamoorti R, Giannelis EP. *Langmuir* 2001;17:1448 -1452
17. Kuppa V, Manias E. *Chem. Mater.* 2002;14:2171-2175
18. Sandi G, Carrado KA, Joachin H, Lu W, Prakash J. *Journal of Power Sources* 2003;119-211:492-496
19. Krawiec W, Scanlon LG, Fellner JP, Vaia RA, Vasudevan S, Giannelis EP. *Journal of Power Sources* 1995;54:310-315
20. Vaia RA, Vasudevan, S, Krawiec W, Scanlon LG, Giannelis EP. *Advanced Materials* 1995;7:154–156
21. Shen Z, Simon GP, Cheng YB. *Polymer* 2002;43:4251-4260
22. Vaia RA, Sauer BB, Tse OK, Giannelis EP. *Journal of Polymer Science: Part B: Polymer Physics* 1997;35:59-67
23. Aranda P, Ruiz-Hitzky E. *Chem. Mater.* 1992;4:1395-403

24. Wu J, Lerner MM. Chem. Mater. 1993;5: 835–838
25. Hackett E, Manias E, Giannelis EP. Chem. Mater. 2000;12:2161-2167
26. Shen Z, Simon GP, Cheng YB. Polymer Engineering and Science 2002;42:2369-2382
27. Choi HJ, Kim SG, Hyun YH, Jhon MS. Macromol. Rapid Commun. 2001;22:320–325
28. Hyun YH, Lim ST, Choi HJ, Jhon MS. Macromolecules 2001;34:8084–8093
29. Ratna D, Divekar S, Samui AB, Chakraborty BC, Banthia AK. Polymer 2006;47:4068-4074
30. Jog JP. Materials Science and Technology 2006;22:797-806
31. Kelarakis A, Yoon K, Sics I, Somani RH, Chen X, Hsiao BS, Chu B. J. Macromolecular Science, Part B: Physics 2006;45:257-261
32. Tseng CR, Wu JK, Lee HY, Chang FC. Polymer 2001;42:10063-10070
33. Lincoln DM, Vaia RA, Wang ZG, Hsiao BS, Krishnamoorti R. Polymer 2001;42:9975-9985
34. Kelarakis A, Hayrapetyan S, Ansari S, Fang J, Estevez L, Giannelis EP. Polymer 2010;51:469-474
35. Chen HW, Chang FC. Polymer 2001;42:9763-9769
36. Ogata N, Kawakage S, Ogihara T. Polymer 1997;38:5115-5118
37. Kelarakis A, Yoon K. European Polymer Journal 2008;44:3941-3945
38. Loyens W, Jannasch P, Maurer FHJ. Polymer 2005;46:903-914
39. Strawhecker KE, Manias E. Chem. Mater. 2003;15:844-849
40. Chatterjee T, Yurekli K, Hadjiev VG, Krishnamoorti R. Adv. Funct. Mater. 2005;15:1832-1838
41. Zheng X, Xu Q. J. Phys. Chem. B 2010;114:9435-9444
42. Chintapalli S, Frech R. Macromolecules 1996;29:3499-3506
43. Croce F, Appetecchi GB, Persi L, Scrosati B. Nature 1998;394:456-458
44. Gadjourova Z, Andreev YG, Tunstall DP, Bruce PG. Nature 2001;412:520
45. Pedersen CJ. Science 1988;241:536-540
46. Hoffmann B, Dietrich C, Thomann R, Friedrich C, Mulhaupt R. Macromol. Rapid Commun. 2000;21:57-61

47. Krishnamoorti R, Yurekli K. *Curr. Opin. Colloid Interface Sci.* 2001;6:464–470
48. Kellarakis A, Yoon K, Somani RH, Chen XM, Hsiao BS, Chu B. *Polymer* 2005;46:11591-11599
49. Kellarakis A, Giannelis EP, Yoon K. *Polymer* 2007;48:7567- 7572
50. Booth C, Devoy CJ. *Polymer* 1971;12: 309-319
51. Unger R, Beyer D, Donth E. *Polymer* 1991;32:3305-3312
52. Choi S, Lee KM, Han CD. *Macromolecules* 2004;37:7649-7662
53. Huang W, Han CD. *Macromolecules* 2006;39:257-267
54. Wang X, Gao Y, Mao K, Xue G, Chen T, Zhu J, Li B, Sun P, Jin Q, Ding D, Shi AC. *Macromolecules* 2006;39:6653-6660
55. Wang X, Sun P, Xue G, Winter HH. *Macromolecules* 2010;43:1901-1906
56. Gelfer MY, Burger C, Chu B, Hsiao BS, Drozdov AD, Si M, Rafailovich M, Sauer BB, Gilman JW. *Macromolecules* 2005;38:3765-3775
57. Xie W, Gao Z, Pan WP, Hunter D, Singh A, Vaia R. *Chem. Mater.* 2001;13: 2979-2990
58. Lee KM, Han CD. *Polymer* 2003;44:4573-4588
59. Lee KM, Han CD. *Macromolecules* 2003;36:804-815
60. Lee KM, Han CD. *Macromolecules* 2003;36:7165-7178
61. Zhang Q, Archer LA. *Langmuir* 2002;18:10435-10442

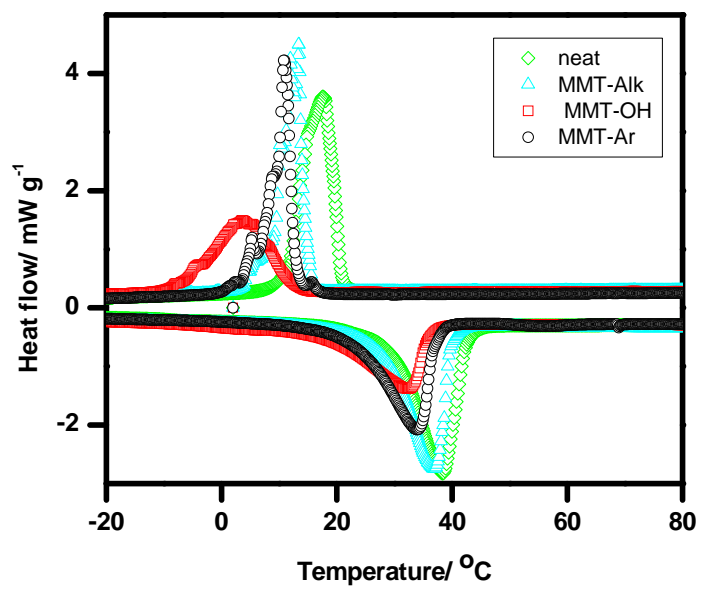


Figure 1

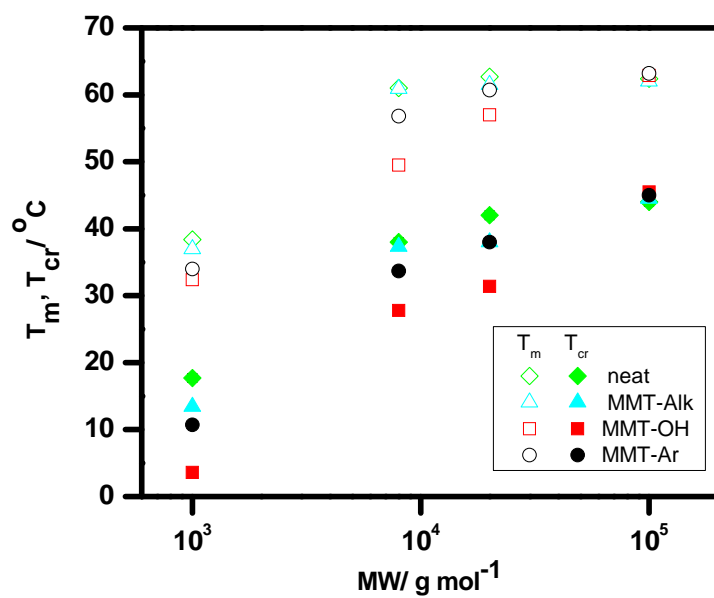


Figure 2

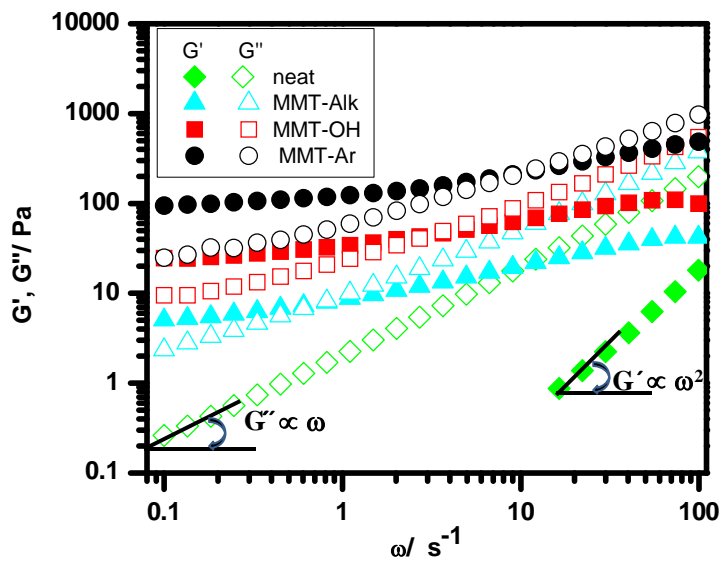


Figure 3

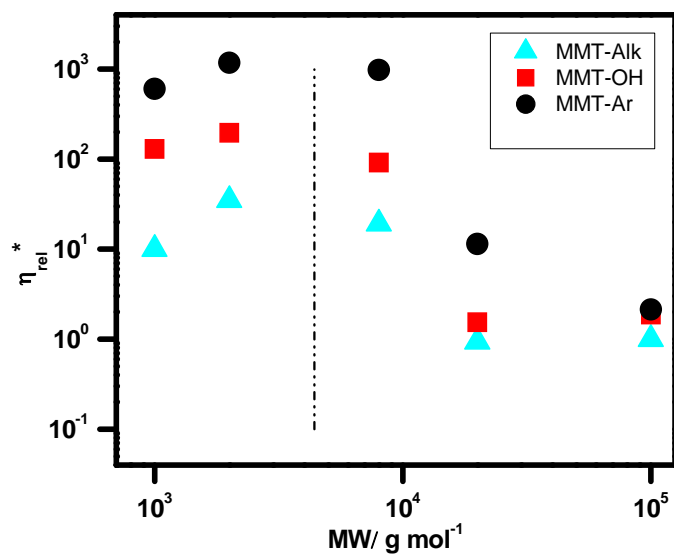


Figure 4

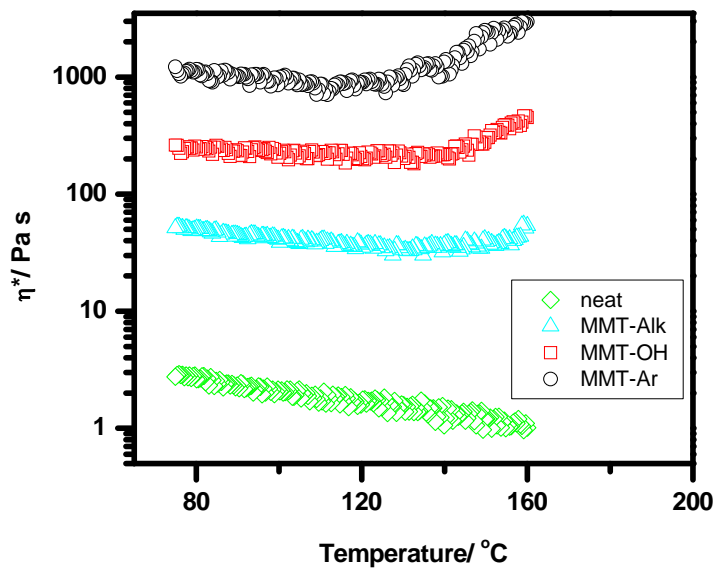


Figure 5

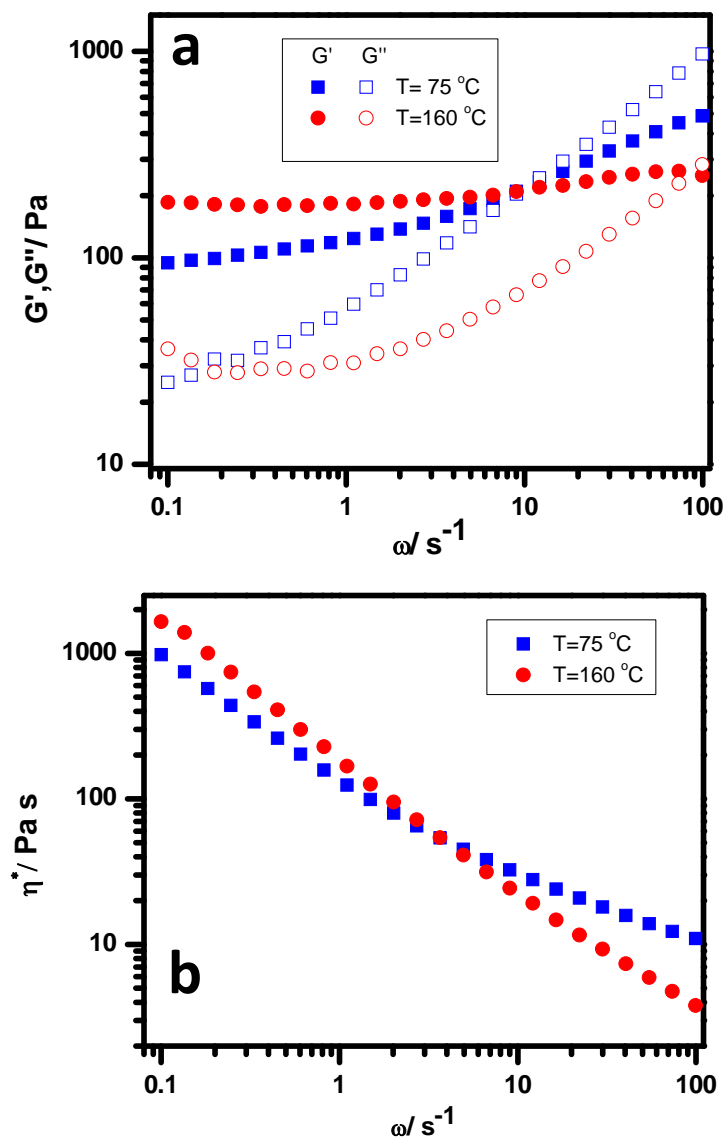


Figure 6

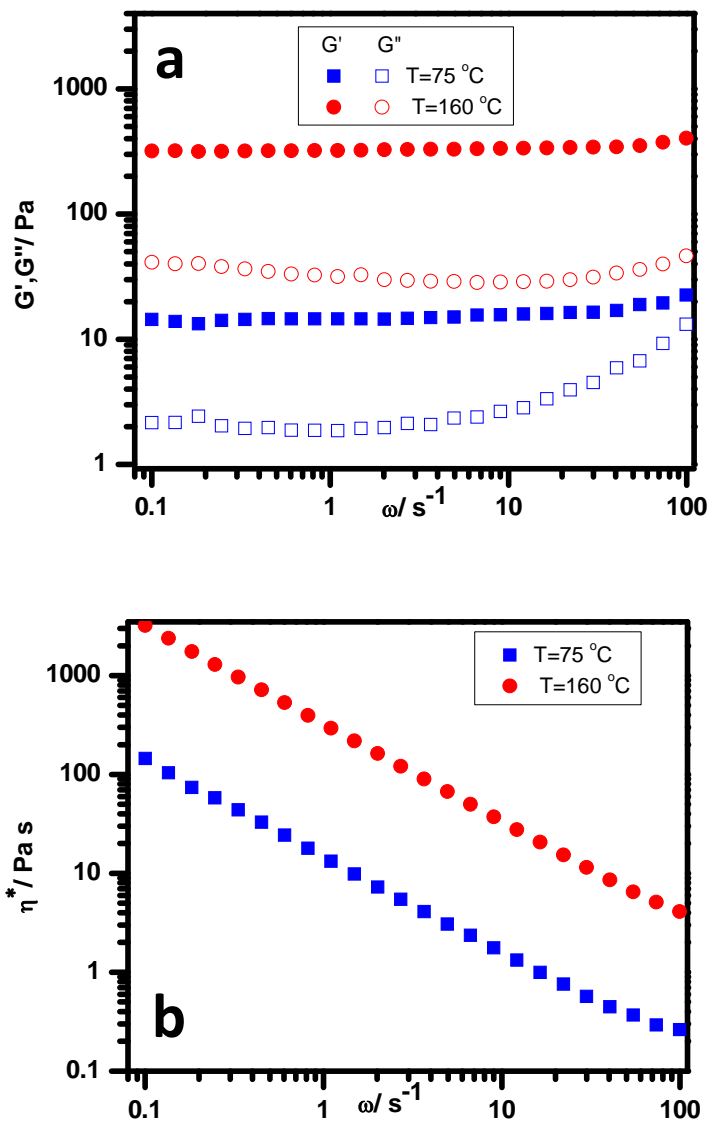


Figure 7

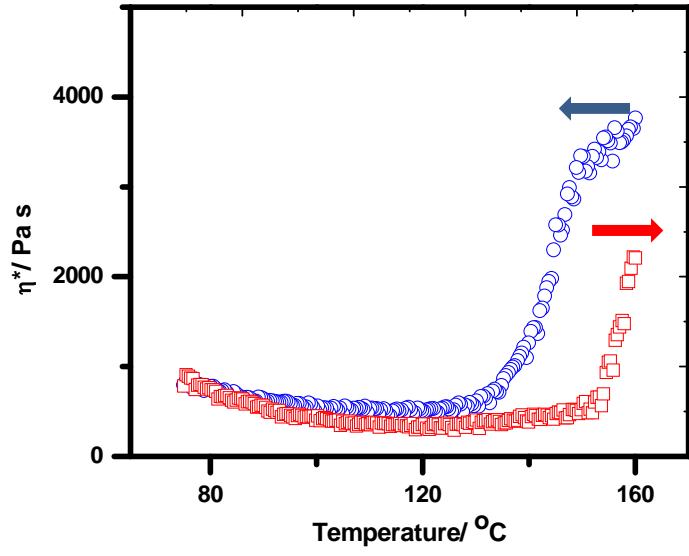


Figure 8